PNAS RESEARCH ARTICLE | MEDICAL SCIENCES

The RNA-binding protein RBPMS inhibits smooth muscle cell–driven vascular remodeling in atherosclerosis and vascular injury

Jianlin Du[a,1], Xin Yuan[b,1], Jiajia Wang[c,1], Lujun Zhang[c], Fangyan Tan[d], Tianyang Hu[c], Xingsheng Li[c], Fan Liu[a,e], Haitao Ran[a,e], Zhigang Wang[a,e], Yongyong Li[c], Yuxing Feng[f], N. D. Melgiri[g], Yu Cao[h], Lihong Jiang[i,j,2], Rongzhong Huang[c,2], and Yang Sun[a,e,2]

Affiliations are included on p. 12.

Edited by Peter Tontonoz, University of California, Los Angeles, CA; received August 6, 2024; accepted January 13, 2025

Atherosclerosis and vessel wall trauma induce vascular smooth muscle cell (VSMC) phenotypic modulation, leading to plaque cap growth and postintervention restenosis. Our systems biology approach identified RNA binding protein, mRNA processing factor (*RBPMS*) as a conserved, VSMC-specific gene associated with VSMC modulation in atherosclerosis. *RBPMS* gene expression positively correlates with VSMC contractile markers in human and murine atherosclerotic arteries as well as in two vascular injury models during the postinjury intimal hyperplasia phase. RBPMS promotes contractile VSMC differentiation, reduces plaque cap development in high-fat diet-fed apolipoprotein E-null (*ApoE*$^{-/-}$) murine atherosclerotic arteries, and inhibits intimal hyperplasia. Mechanistically, the RBPMS protein interacts with the myocardin (*MYOCD*) pre-mRNA and enhances *MYOCD_v3*/*MYOCD_v1* transcript balance through alternative exon 2a splicing. RBPMS promotes the VSMC contractile phenotype and reduces their fibroproliferative activity in a MYOCD_v3a-dependent manner. RBPMS enhances *Myocd_v3*/*Myocd_v1* transcript balance in both atherosclerotic and injured vessels. RBPMS may inhibit VSMC-driven plaque cap development and intervention-induced restenosis.

atherosclerosis | vascular injury | smooth muscle cell | RBPMS | MYOCD

Significance

An improved understanding of the mechanisms driving vascular smooth muscle cell (VSMC) modulation in the diseased vessel wall is needed to improve our approach to atherosclerotic plaque cap development and intervention-induced restenosis. The RNA-binding protein, mRNA processing factor (RBPMS) inhibits VSMC modulation and maintains VSMCs in a differentiated, contractile state by regulating the expression and alternative pre-mRNA splicing of the VSMC master regulator myocardin. This evidence suggests that RBPMS may play a role in inhibiting VSMC-driven plaque cap development and intervention-induced restenosis.

Atherosclerotic cardiovascular disease is the leading cause of morbidity and mortality globally (1). The atherosclerotic disease process, as well as vessel wall trauma from percutaneous interventions applied to treat atherosclerotic disease, induces vascular smooth muscle cells (VSMCs) to dedifferentiate from their contractile phenotype into a modulated VSMC phenotype (2–4). This phenotypic modulation results in VSMC hyperproliferation, migration, and deposition of excessive extracellular matrix. This process leads to plaque cap development and postintervention vascular restenosis that hinders the long-term efficacy of percutaneous interventions (3–5). There are limited clinical options available to address this issue, particularly for recurrent post–stent restenosis patients. Despite advances in drug-eluting stent technologies, post–stent restenosis rates remain at approximately 5 to 10% (6). Given that modulated VSMCs are estimated to comprise approximately 30% of all cells within atherosclerotic plaques (7), a better understanding of the mechanisms driving VSMC modulation in the diseased vessel wall is needed to improve our approach to plaque cap development and intervention-induced restenosis.

Here, using single-cell RNA sequencing (scRNAseq) data from high-fat diet (HFD)-fed *ApoE*$^{-/-}$ murine atherosclerotic arteries and human atherosclerotic coronary arteries, we identified *RBPMS* (which encodes RNA binding protein, mRNA processing factor; HERMES) as a conserved, VSMC-specific gene positively associated with contractile VSMC differentiation in atherosclerosis. Employing a systems biology workflow, bioinformatics findings on *RBPMS* dysregulation from three independent human atherosclerotic biobanks were carried forward to functional investigations on RBPMS in animal models of atherosclerosis and acute vascular injury as well as in vitro mechanistic studies on RBPMS in human VSMCs. We demonstrate that RBPMS inhibits VSMC modulation and maintains VSMCs in a differentiated, contractile state by regulating the gene expression and alternative pre-mRNA splicing of the VSMC master regulator myocardin (*MYOCD*). The evidence presented here suggests that RBPMS may play a role in inhibiting VSMC-driven plaque cap development and intervention-induced restenosis.

Results

***Rbpms* Gene Expression Is Positively Associated with Contractile VSMC Differentiation in Murine and Human Atherosclerotic Arteries.** We performed scRNAseq analyses on published scRNAseq data (GEO acc. no.: GSE131776) derived from Fluorescence

Author contributions: H.R., Z.W., R.H., and Y.S. designed research; J.D., X.Y., J.W., L.Z., F.T., T.H., F.L., Y.C., R.H., and Y.S. performed research; X.Y., J.W., L.Z., X.L., Y.L., Y.F., Y.C., L.J., R.H., and Y.S. contributed new reagents/analytic tools; J.D., X.Y., J.W., T.H., X.L., Y.C., and R.H. analyzed data; and J.D., N.D.M., R.H., and Y.S. wrote the paper.

The authors declare no competing interest.

This article is a PNAS Direct Submission.

[1]J.D., X.Y., and J.W. contributed equally to this work.

[2]To whom correspondence may be addressed. Email: xw2015103@kust.edu.cn, rzhuang@hospital.cqmu.edu.cn, or sunyang@cqmu.edu.cn.

This article contains supporting information online at https://www.pnas.org/lookup/suppl/doi:10.1073/pnas.2415933122/-/DCSupplemental.

Published February 25, 2025.

activated cell sorting (FACS)-sorted cells from the ascending aorta and aortic root of *ApoE*$^{-/-}$ BAC transgenic mice. These transgenic mice express a tamoxifen-inducible Cre recombinase under the control of an SMC-specific smooth muscle myosin heavy chain (*Myh11*) promoter and a Cre-responsive tandem dimer Tomato reporter gene (*tdT*) inserted at the *Rosa26* locus (*Rosa*$^{tdT/+}$). Therefore, when these transgenic mice were dosed tamoxifen at the age of 8 wk (baseline), all SMC lineage cells and any progeny therefrom were labeled with a tdT fluorescent marker.

Cell type–specific marker genes were employed to identify and discriminate between the major cell types at baseline (*SI Appendix*, Fig. S1*A*), and we confirmed that the SMC lineage (tdT+) cells mapped to the SMC clusters (*SI Appendix*, Fig. S1*B*). Contractile SMCs and modulated SMCs were present at baseline (Fig. 1*A*). The SMC/fibroblast clusters were tracked from baseline, to 8 wk of HFD, and 16 wk of HFD in order to track changes coincident with HFD-induced atherogenesis (Fig. 1*B*). Consistent with Wirka et al.'s findings (2), we observed an increase in the proportion of modulated SMCs coupled with a decrease in the proportion of contractile SMCs from baseline to 16 wk of HFD (Fig. 1*C*). We then analyzed differential gene expression between modulated SMCs and contractile SMCs. We identified 765 and 976 differentially expressed genes (DEGs) (adj. $P < 0.05$) after 8 and 16 wk of HFD, respectively. When considering both time points together, there were a total of 952 DEGs differentiating modulated SMCs from contractile SMCs that were significantly enriched for mitochondrial complex I assembly and protein folding processes (Dataset S1). The most upregulated DEGs and most downregulated DEGs in modulated SMCs by fold-change are respectively displayed in *SI Appendix*, Fig. S2 *A* and *B*.

To assess whether our findings from the murine atherosclerosis model are mirrored in human atherosclerosis patients, we conducted

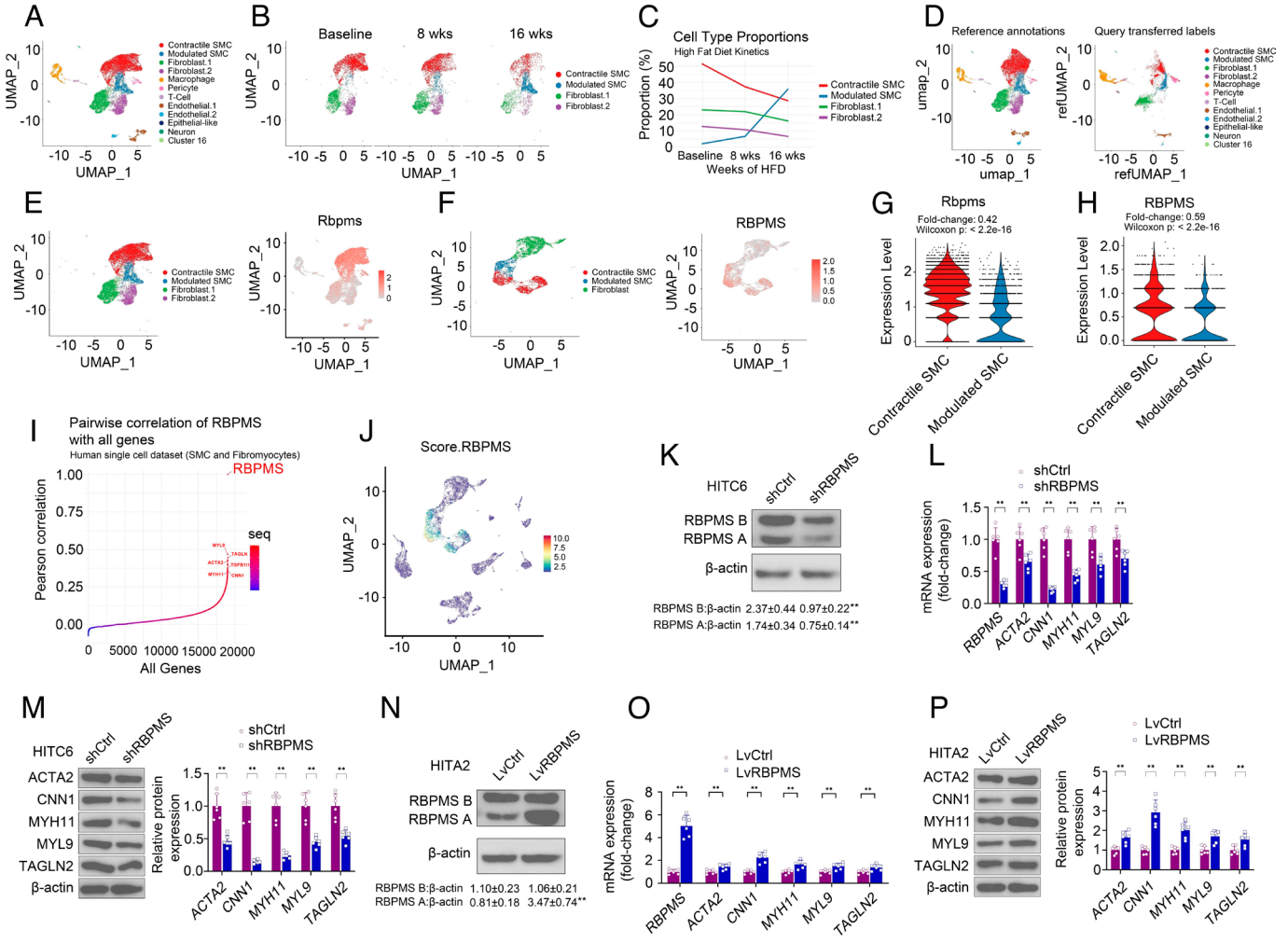

Fig. 1. *Rbpms* positively associated with contractile VSMC differentiation in murine and human atherosclerotic arteries. (*A*–*H*) scRNAseq analyses on data from FACS-sorted cells derived from the ascending aorta and aortic root of *ApoE*$^{-/-}$ BAC transgenic mice (GSE131776) and dissociated cells derived from nonstented, diseased right coronary artery segments of four human heart transplant recipients (GSE131778). (*A* and *B*) Uniform Manifold Approximation and Projection (UMAP) plots illustrating (*A*) all major cell types (cell clusters) within murine aortic roots at baseline and (*B*) the VSMC/fibroblast clusters at baseline, after 8 wk, and after 16 wk of HFD. (*C*) Percentage (%) of each VSMC/fibroblast cluster by cell count within murine aortic roots at baseline, after 8 wk, and after 16 wk of HFD. (*D*) Seurat package-based joint clustering of murine and human datasets using canonical correlation analysis. The joint murine/human clusters were mapped back onto the human dataset. The UMAP plots depict the two datasets [mouse (*Right*) and human (*Left*)] mapped onto the same UMAP space ("Unimodal UMAP Projection"), so they can be directly compared. (*E* and *F*) UMAP plots illustrating *Rbpms* expression across the VSMC/fibroblast clusters from (*E*) the mouse dataset and (*F*) human dataset. (*G* and *H*) Violin plots comparing *Rbpms* expression in the contractile VSMC ("VSMC") cluster vs. the "modulated VSMC" cluster from (*G*) the mouse dataset and (*H*) human dataset. (*I*) Pairwise Pearson correlation of *RBPMS* with every other gene in cells across the "VSMC" and "modulated VSMC" clusters in the human dataset. Selected examples of genes regulated during VSMC modulation are labeled. (*J*) The 20 most positively correlated and 20 most negatively correlated genes from panel (*I*) were used to calculate an "*RBPMS* score." UMAP plot illustrating the "*RBPMS* scores" for the cell clusters within the human dataset. (*K*–*P*) Modulation of key contractile VSMC marker gene expression in *K*–*M* HITC6 VSMCs following stable ShRBPMS or shCtrl transduction or (*N*–*P*) HITA2 VSMCs following *RBPMS* cDNA overexpression vector (LvRBPMS) or control overexpression vector (LvCtrl) transduction ($n = 6$ biological replicates/group). Data represented as means ± SDs. *$P < 0.05$, **$P < 0.01$ [(*G* and *H*) Wilcoxon signed-rank test; (*I*) Pairwise Pearson correlation; (*K*–*P*) unpaired two-tailed *t*-test].

analogous scRNAseq analyses on data from dissociated cells derived from nonstented, diseased right coronary artery segments of four human heart transplant recipients (GEO acc. no.: GSE131778). As in the mouse model, cell type–specific marker genes were employed to identify and discriminate between the major cell types (*SI Appendix*, Fig. S3 *A* and *B*). In addition, an integration strategy based on principal component analysis was used to project the afore-described mouse cell type reference profiles onto the human dataset. We found that this approach accurately clustered together the known orthologous cell types (Fig. 1*D*). Employing these projected categories, we identified 609 DEGs (343 up- and 266 down-regulated; adj. $P < 0.05$) differentiating human modulated SMCs from contractile SMCs that were significantly enriched for mRNA processing and RHO GTPase-associated pathways (Dataset S2).

In order to identify gene candidates for further investigation, we applied the following criteria: a DEG identified from both the mouse and human comparisons, absolute fold-change >1.5, and a >30% difference in the proportion of cells expressing the gene in both conditions. These selection criteria produced 49 DEG candidates (34 up- and 15 down-regulated DEGs in contractile SMCs) (*SI Appendix*, Fig. S4 *A* and *B*). We then limited this DEG set to transcription factors (TFs) or their cofactors (coTFs), as TFs/coTFs DEGs would likely have a more profound influence on SMC differentiation. This produced four DEG candidates (*HSPA1A*, *RBPMS*, *TGFB1*, *TGFB1I1*), *TGFB1* being downregulated and the other three being upregulated in contractile SMCs (*SI Appendix*, Fig. S5 *A* and *B*). Given that *HSPA1A* and TGF-β signaling factors have been previously linked to atherosclerosis (8, 9), we opted to investigate *RBPMS*.

We analyzed *RBPMS* gene expression in all major cell types from the mouse dataset (Fig. 1*E*) and human dataset (Fig. 1*F*), which revealed *RBPMS* enrichment in the contractile SMC clusters. *RBPMS* expression was significantly upregulated in contractile SMCs relative to modulated SMCs in both species (Fig. 1 *G* and *H*). To determine whether *RBPMS* was associated with contractile SMC differentiation, we performed pairwise Spearman correlation analyses between *RBPMS* and every other gene expressed in the SMC lineage clusters in the mouse and human datasets. We found that *RBPMS* was highly correlated with contractile SMC markers in humans (Fig. 1*I*) and mice (Dataset S3). We visualized the behavior of the *RBPMS*-associated transcriptional program within the human cell populations by creating an *RBPMS* score for each cell (*Materials and Methods*), which reflected the average expression of the top *RBPMS*-correlated genes across the SMC lineage clusters. This analysis revealed a graded increase in the *RBPMS*-associated gene expression program that correlated with contractile SMC differentiation (Fig. 1*J*).

The RBPMS protein sequence (*SI Appendix*, Fig. S6*A*), protein–protein interaction network (*SI Appendix*, Fig. S6*B*), and top-ranked Gene Ontology biological processes (GO-BP) (most notably RNA splicing and mRNA processing, *SI Appendix*, Fig. S6*C*) are highly conserved among humans, mice, and rats. This evidence implies strong conservation of RBPMS's function across these species. To determine whether RBPMS promotes contractile SMC differentiation in vitro, we conducted a set of experiments in two human VSMC clonal cell lines. The HITC6 VSMC line, which expresses relatively high levels of RBPMS and contractile apparatus proteins (10) (*SI Appendix*, Fig. S7), was used to assess the effects of shRNA-based *RBPMS* knockdown using an *RBPMS* shRNA (shRBPMS) or control shRNA (shCtrl). Upon silencing of *RBPMS* (Fig. 1*K*), we accordingly found downregulation of these contractile VSMC markers (Fig. 1 *L* and *M*). The HITA2 VSMC line, which expresses relatively low levels of RBPMS and contractile apparatus proteins (10) (*SI Appendix*, Fig. S6), was used to assess the effects of lentiviral-mediated overexpression of the active RBPMS isoform RBPMS-A in VSMCs (11). Upon overexpression of RBPMS-A (Fig. 1*N*), we found upregulation of several key contractile VSMC markers (Fig. 1 *O* and *P*). This combined evidence suggests that RBPMS may promote contractile VSMC differentiation in the vascular wall and thereby impact atherogenesis.

***Rbpms* Gene Expression Is Downregulated in Atherosclerotic Plaques and Positively Associated with Contractile VSMC Markers.** In order to investigate *RBPMS* dysregulation in atherosclerotic plaques, we chose to analyze human atherosclerotic carotid plaque data for two reasons. First, there are significantly larger number of samples in the publicly available atherosclerotic carotid plaque datasets relative to the publicly available atherosclerotic coronary artery datasets. Second, atherosclerotic carotid samples possess an internal matched control (i.e., central plaque segment vs. distal nonplaque segment). Atherosclerotic coronary artery datasets typically possess noncoronary control arteries (i.e., internal mammary artery, mesenteric artery), which may not be as reliable. We analyzed *RBPMS* mRNA expression in human atherosclerotic carotid plaques using three publicly available transcriptomic datasets (GEO acc. nos.: GSE43292, GSE163154 (MaasHPS), and GSE111782). Respectively, *RBPMS* expression was downregulated in central relative to distal carotid tissue, in intraplaque hemorrhage (IPH) relative to non-IPH carotid plaques, and in symptomatic relative to asymptomatic carotid atheroma patients (Fig. 2*A*). We also examined *RBPMS* mRNA expression in carotid samples derived from our cohort of hypertensive carotid atheroma patients (n = 20 patients, *SI Appendix*, Table S1) that underwent multicontrast magnetic resonance carotid wall imaging for IPH and disrupted plaque surface [DPS, defined as ulceration and/or fissured fibrous cap (12)] prior to carotid endarterectomy. *RBPMS* was significantly downregulated in central relative to distal carotid tissue, in IPH plaques relative to non-IPH plaques, and in DPS plaques relative to non-DPS plaques (Fig. 2*B*). This evidence suggests that RBPMS downregulation may be associated with atherogenesis and plaque instability.

We correlated *RBPMS* mRNA expression with contractile VSMC marker expression in our central carotid plaque cohort (Fig. 2*C*). *RBPMS* showed strong positive correlations with all contractile VSMC markers (i.e., *ACTA2*, *CNN1*, *MYH11*, *MYL9*, and *TAGLN2*). As TAGLN (SM22α) is a VSMC marker whose expression is resistant to atherosclerosis-induced changes (13), we used it as a pan-VSMC marker for IHC analyses. We found a significantly lower RBPMS+ VSMC percentage in central carotid plaques relative to distal carotid tissue (Fig. 2*D*). To verify these findings, early-passage cultured VSMCs from central carotid plaques and distal carotid tissue (n = 6 randomly selected samples per cohort) were interrogated for RBPMS mRNA and protein expression. Central carotid plaque VSMCs displayed lower RBPMS mRNA and protein expression relative to distal carotid VSMCs (Fig. 2 *E* and *F*). To verify our findings in atherosclerotic mice, lower *Rbpms* mRNA expression and a lower RBPMS+ VSMC percentage were confirmed in aortic root plaques from 16-wk HFD-fed $ApoE^{-/-}$ mice relative to aortic root tissue from chow-fed $ApoE^{-/-}$ mice (Fig. 2 *G* and *H*). Similar to human plaques, *Rbpms* showed strong positive correlations with all contractile VSMC markers in murine aortic root plaques (Fig. 2*I*).

***Rbpms* Gene Expression Is Downregulated Postvascular Injury and Positively Associated with Contractile VSMC Markers.** Similar to atherosclerosis, acute vascular injury also produces VSMC modulation and resulting intimal hyperplasia (14). This

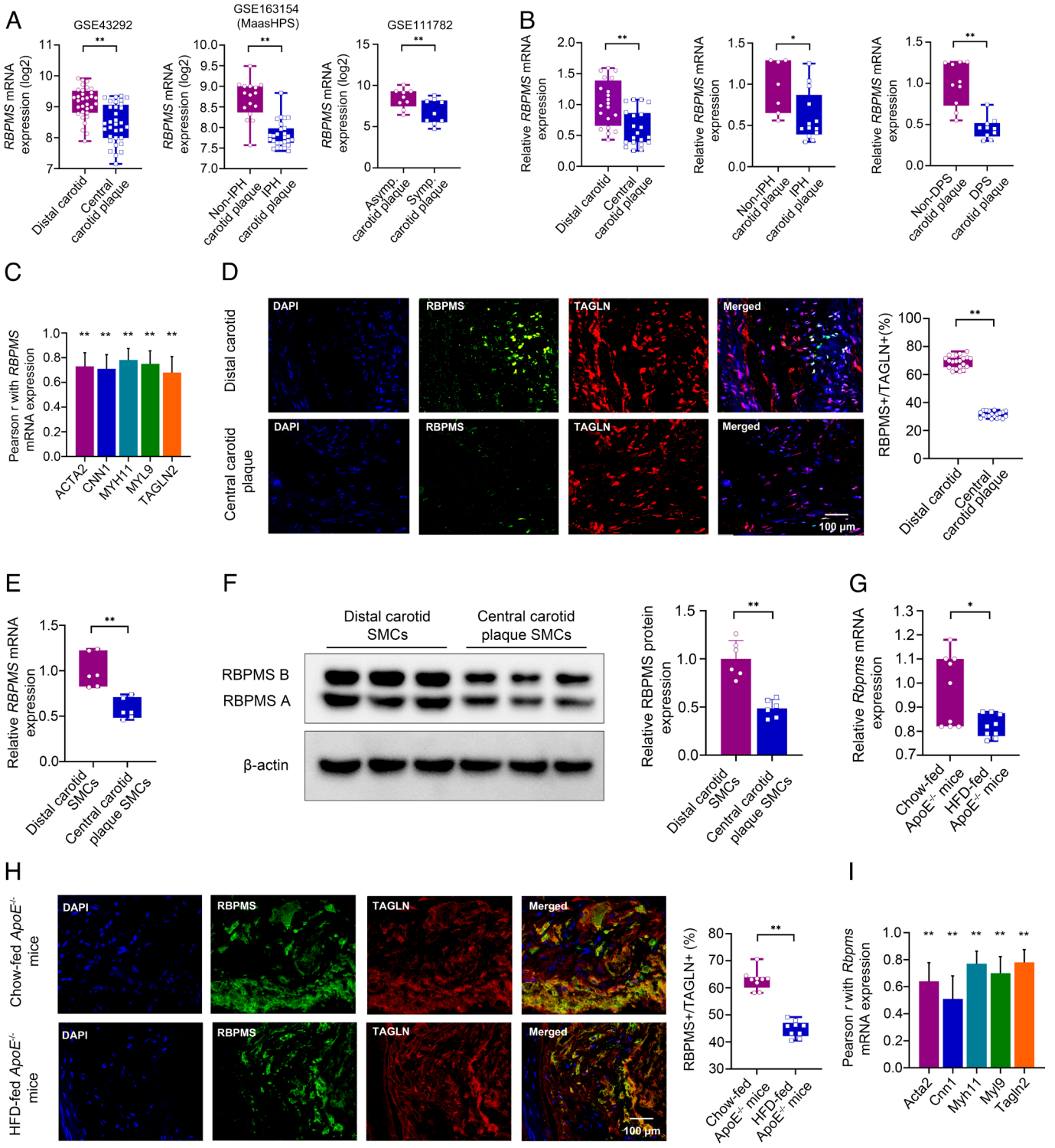

Fig. 2. *Rbpms* downregulated in atherosclerotic plaque VSMCs from mice and humans. (*A*) Analyses of *RBPMS* mRNA expression (log_2) in the human atherosclerotic carotid plaque transcriptomic datasets [GEO acc. nos.: GSE43292, GSE163154 (MaasHPS), and GSE111782]. IPH: intraplaque hemorrhage. (*B–F*) The following analyses were performed on carotid samples derived from our cohort of hypertensive carotid atheroma patients (n = 20). (*B*) Analyses of *RBPMS* mRNA expression by plaque status, IPH status, and DPS status. (*C*) Pearson correlations between *RBPMS* mRNA expression and various contractile VSMC markers in central carotid plaques. (*D*) Representative immunohistochemical images showing RBPMS+ cells (brown) and TAGLN (SM22α)+ cells (blue). (Scale bar, 100 μm.) Quantification of RBPMS+ VSMC percentages (RBPMS+ cells/TAGLN+ cells × 100%) in central carotid plaques vs. matched distal carotid tissue. (*E* and *F*) Analyses of (*E*) *RBPMS* mRNA expression and (*F*) RBPMS protein expression in actively dividing VSMCs derived from central plaques vs. matched distal tissue. (*G–I*) The following analyses were performed on aortic plaque samples from HFD-fed vs. chow-fed *ApoE*$^{-/-}$ mice (n = 9 mice/cohort). (*G*) qPCR of *Rbpms* mRNA expression. (*H*) Representative immunohistochemical images showing RBPMS+ cells (brown) and TAGLN (SM22α)+ cells (blue) (Scale bar, 50 μm.) and quantification of RBPMS+ VSMC percentages (RBPMS+ cells/TAGLN+ cells × 100%). (*I*) Pearson correlations between *Rbpms* mRNA expression and various contractile VSMC markers. Data represented as means ± SDs or IQRs ± ranges. *$P < 0.05$, **$P < 0.01$ [(*A*, *B*, *D*, *E*, *G*, and *H*) Mann–Whitney *U* test; (*C* and *I*) Pearson correlation; (*F*) paired two-tailed *t*-test].

led us to investigate *Rbpms* dysregulation in two animal models of acute vascular injury: a rat carotid arterial injury model and a murine femoral arterial hyperplastic model. In these models, contractile VSMC marker levels within the vessel wall elevate during the first 1 to 2 d postinjury but then decline during the intimal hyperplasia phase thereafter. In the rat carotid arterial injury model,

injured carotid tissue showed brief upregulated *Rbpms* expression (days 1 to 3) followed by downregulated *Rbpms* expression (days 7 to 14) (*SI Appendix*, Fig. S8*A*). The murine femoral arterial hyperplastic model displayed a similar temporal pattern of *Rbpms* expression: brief upregulated *Rbpms* expression (day 1) followed by downregulated *Rbpms* expression (days 3 to 14) (*SI Appendix*, Fig. S8*B*). These data indicate that *Rbpms* gene expression is briefly upregulated postinjury but then downregulated during the intimal hyperplasia phase post–vascular injury.

In order to elucidate the VSMC pathway(s) regulated by *Rbpms*, we conducted a transcriptomics analysis on the global transcriptomes of rat VSMCs with siRNA-induced *Rbpms* knockdown (*Rbpms* KD) vs. control rat VSMCs (GEO acc. no.: GSE127799). We performed a Cemi analysis using CemiTool package in R that identified two distinct coexpression gene modules M1 and M2 (*SI Appendix*, Fig. S8*C*). The 121-member M1 module was positively associated with *Rbpms* KD [net enrichment score (NES) = 4.16] and was significantly enriched for several Reactome mRNA translation pathways, most notably "SRP-dependent cotranslational protein targeting to membrane," "Nonsense mediated decay independent of the exon junction complex", and "Formation of a pool of free 40S subunits" (*SI Appendix*, Figs. S8 *C* and *D* and S9). The 48-member M2 module was negatively associated with *Rbpms* KD (NES = −2.51) and was significantly enriched for several Reactome metabolic pathways, most notably "Gluconeogenesis," "Glycolysis," and "Glucose metabolism" (*SI Appendix*, Figs. S8 *C* and *D* and S9). Our DEG analysis revealed 722 up- and 374 down-regulated DEGs in *Rbpms* KD VSMCs (Dataset S4), with M1 module DEGs (n = 8) all being upregulated and M2 module DEGs (n = 11) being predominantly downregulated (*SI Appendix*, Fig. S8 *E* and *F*). The follow-up linear regression analysis revealed that all M1 module DEGs and M2 module DEGs were significantly correlated with *Rbpms* (*SI Appendix*, Fig. S8*G*).

In cultured rat carotid VSMCs subjected to siRNA-induced *Rbpms* KD (*SI Appendix*, Fig. S10 *A* and *B*), qPCR validation confirmed downregulation of several contractile VSMC markers identified from the foregoing DEG analysis (*SI Appendix*, Fig. S10*C*). To validate these findings under conditions of vascular injury in vivo, we analyzed the correlations of *Rbpms* with the afore-described qPCR-validated DEGs in injured tissue samples from the rat carotid arterial injury model and murine femoral arterial hyperplastic model at day 3 and day 1, the respective points of maximal *Rbpms* expression in these models. We identified significant correlations between *Rbpms* and several VSMC contractile markers in both models (*SI Appendix*, Fig. S10 *D* and *E*). This evidence indicates that *Rbpms* gene expression is positively associated with contractile VSMC markers post–vascular injury.

Platelet-Derived Growth Factor (PDGF)-BB Downregulates *RBPMS* Gene Expression Through Promoting ELK1 Phosphorylation. Given that *Rbpms* gene expression is associated with contractile VSMCs and is downregulated in atherosclerotic plaques and vascular injury, we aimed to identify the physiologic signal(s) that drive *Rbpms* downregulation in VSMCs. Vascular injury is known to induce various growth factors that affect VSMCs (15). Among these factors, PDGF-BB is considered the key growth factor driving VSMC phenotypic modulation in injured vessels. Mechanistically, vascular injury-induced PDGF-BB, through its receptor PDGFRβ, promotes MAPK-mediated phosphorylation of ETS-like transcription factor-1 (ELK1→p-ELK1^{S383}) (16, 17). p-ELK1^{S383} competitively displaces MYOCD from the serum response factor (SRF)-MYOCD transcription factor complex to form the SRF-p-ELK1^{S383} transcription factor complex. As the SRF-MYOCD complex supports *RBPMS* gene expression in VSMCs (18), we hypothesized that PDGF-BB downregulates *RBPMS* gene expression through promoting ELK1^{S383} phosphorylation, which displaces MYOCD from the SRF-MYOCD complex.

In HITC6 VSMCs, PDGF-BB upregulated ELK1^{S383} phosphorylation and SRF-p-ELK1^{S383} binding while downregulating SRF-MYOCD binding (*SI Appendix*, Fig. S11*A*) as well as RBPMS mRNA and protein expression (*SI Appendix*, Fig. S11 *B* and *C*). Notably, addition of the PDGFRβ inhibitor imatinib or the ELK1 phosphorylation inhibitor AZD6244 abrogated all these PDGF-BB-induced effects. Moreover, untreated HITC6 VSMCs with lentiviral-mediated overexpression of the ELK1 phosphomimetic ELK1^{S383E} (but not the phospho-dead mutant ELK1^{S383A}) displayed upregulated SRF-p-ELK1^{S383} binding, downregulated SRF-MYOCD binding (*SI Appendix*, Fig. S11*D*), and downregulated RBPMS expression (*SI Appendix*, Fig. S11 *E* and *F*). To correlate these findings in our carotid plaque cohort, early-passage cultured VSMCs from central carotid plaques and distal carotid tissue (n = 20) were subjected to ELISA for p-ELK1^{S383} and RBPMS. Central carotid plaque VSMCs displayed higher p-ELK1^{S383} expression and lower RBPMS expression relative to distal carotid VSMCs (*SI Appendix*, Fig. S11*G*). Moreover, expression levels of p-ELK1^{S383} and RBPMS in central carotid plaque VSMCs were negatively correlated (r = −0.66, P < 0.01) (*SI Appendix*, Fig. S11*H*). These findings indicate that PDGF-BB-induced ELK1^{S383} phosphorylation downregulates *RBPMS* gene expression in VSMCs.

RBPMS Reduces Atherosclerotic Plaque Cap Development in *ApoE*$^{-/-}$ Mice. To assess the role of RBPMS in atherosclerotic plaque cap development, we performed studies on atherosclerotic aortic root and ascending aorta samples from VSMC-specific *Rbpms*-overexpressing mice on an *ApoE*$^{-/-}$ background (*ApoE*$^{-/-}$;*Rbpms*-Tg) and matching control mice (*ApoE*$^{-/-}$;Ctrl-Tg) after 16 wk of HFD (Fig. 3*A*). *ApoE*$^{-/-}$;*Rbpms*-Tg mice express a tdT-tagged *Rbpms* transgene under the control of a minimal *TAGLN* (SM22α) promoter, while *ApoE*$^{-/-}$;Ctrl-Tg mice express a tdT-tagged scrambled control sequence under the control of the same promoter. The minimal *TAGLN* promoter is a CC(A/T)6GG DNA binding motif (CArG)-box deleted *TAGLN* promoter that is activated in VSMCs and is not significantly affected by phenotypic modulation (19), making it a stable promoter construct for VSMCs. Therefore, all VSMCs and any progeny therefrom were labeled with a tdT fluorescent marker and sortable by FACS (Fig. 3*B*). We confirmed VSMC-specific *Rbpms* overexpression in VSMC lineage (tdT+) cells from *ApoE*$^{-/-}$;*Rbpms*-Tg murine aortic root samples (Fig. 3*C*). No significant differences in blood pressure, organ weights, peripheral blood cell counts, serum lipids, or serum cytokines were observed between *ApoE*$^{-/-}$;*Rbpms*-Tg mice and controls at 16 wk of HFD (*SI Appendix*, Table S2).

Oil Red O staining of descending aorta revealed similar plaque formation between *ApoE*$^{-/-}$;*Rbpms*-Tg and *ApoE*$^{-/-}$;Ctrl-Tg mice (Fig. 3*D*). Average plaque areas in the aortic root were similar between *ApoE*$^{-/-}$;*Rbpms*-Tg and *ApoE*$^{-/-}$;Ctrl-Tg mice (Fig. 3*E*). Notably, *ApoE*$^{-/-}$;*Rbpms*-Tg plaques displayed reduced cap/plaque and cap/core ratios (Fig. 3 *F*–*H*), suggesting reduced fibroproliferative VSMC activity (19). *ApoE*$^{-/-}$;*Rbpms*-Tg plaques displayed a larger medial area (Fig. 3*I*). *ApoE*$^{-/-}$;*Rbpms*-Tg mice displayed a lower overall plaque VSMC (tdT+ cell) percentage compared to controls (Fig. 3*J*), despite similarly sized tdT+ areas within the entire vessel wall (Fig. 3*K*). *ApoE*$^{-/-}$;*Rbpms*-Tg mice also displayed a lower plaque VSMC percentage within their fibrous caps (Fig. 3*L*). Consistent with the plaque cap phenotype, *ApoE*$^{-/-}$;*Rbpms*-Tg aortic root VSMCs displayed lower levels of the proliferation markers

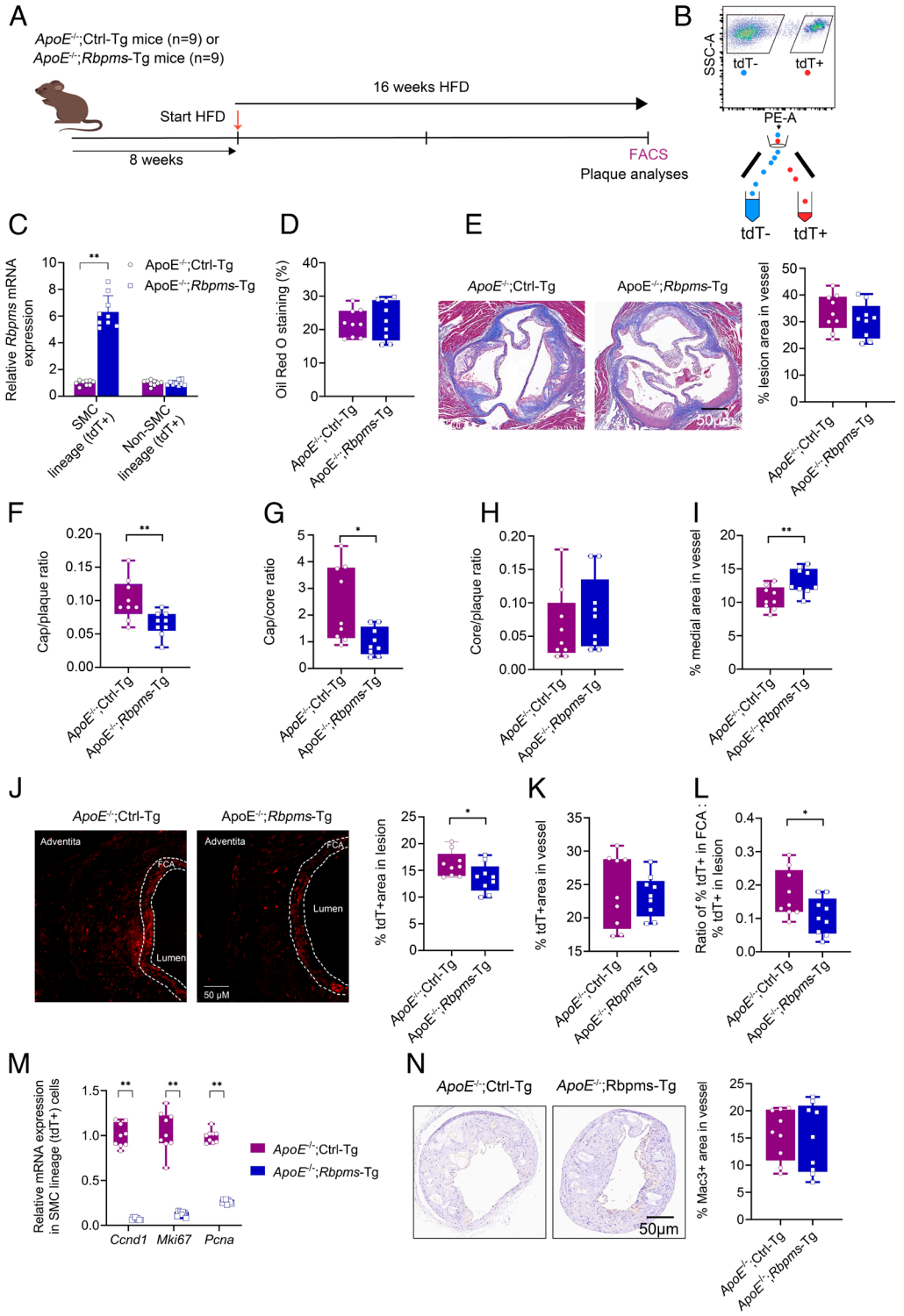

Fig. 3. RBPMS reduces atherosclerotic plaque cap development in $ApoE^{-/-}$ mice. (*A*) VSMC-specific *Rbpms*-overexpressing mice on an $ApoE^{-/-}$ background ($ApoE^{-/-}$;*Rbpms*-Tg) and matching control mice ($ApoE^{-/-}$;Ctrl-Tg) were maintained on a standard chow diet from birth until the age of 8 wk. Mice were then initiated on a HFD and killed following 16 wk of HFD (n = 9 mice/cohort). (*B*) FACS for isolating VSMC lineage (tdT+) cells and non-VSMC lineage (tdT−) cells from murine aortic root samples. (*C*) *Rbpms* expression in VSMC lineage (tdT+) cells and non-VSMC lineage (tdT−) cells from murine aortic root samples. (*D*) Quantification of Oil Red O (ORO)-positive area in the descending aorta. (*E–L*) The following plaque analyses were performed on aortic root sections. (*E*) Representative images of murine aortic root lesions (Scale bar, 50 μm.) and quantification of aortic root lesion area as a % of total aortic root vessel area. (*F–H*) Analyses of the (*F*) cap area/plaque area ratio, (*G*) cap area/necrotic core area ratio, and (*H*) necrotic core area/plaque area ratio. (*I*) Quantification of the medial layer area as a % of total aortic root vessel area. (*J*) Representative images of tdT+ cells (red) in murine aortic root samples (Scale bar, 50 μm.) and percentage of tdT+ staining area in the lesion area. (*K*) Quantification of tdT+ staining area as a % of total aortic root vessel area. (*L*) Ratio of the % tdT+ staining area in the fibrous cap area (FCA, defined as the lesion area within 30 μm of the luminal surface) to the tdT+ staining area in the total aortic root vessel area. (*M*) qPCR of *Ccnd*, *Mki67*, and *Pcna* mRNA expression in tdT+ cells from murine aortic root samples. (*N*) Quantification of the Mac3+ staining area as a % of total aortic root vessel area. Data represented as means ± SDs or IQRs ± ranges. $*P < 0.05$, $**P < 0.01$ [(*C*) two-way ANOVA; (*D–N*) Mann–Whitney *U* test].

Ccnd1, *Mki67*, and *Pcna* (Fig. 3*M*). To account for any effects from vessel macrophage content, we stained the vessels for the macrophage marker Mac3 and found no significant differences between $ApoE^{-/-}$;*Rbpms*-Tg and $ApoE^{-/-}$;Ctrl-Tg mice (Fig. 3*N*).

We performed a similar study in tamoxifen-inducible VSMC-specific *Rbpms*-knockout mice on an $ApoE^{-/-}$ background ($ApoE^{-/-}$;$Rbpms^{fl/fl}$*Tagln-Cre*^{ERT2}; hereinafter $ApoE^{-/-}$;*Rbpms*-KO) and matching $ApoE^{-/-}$;$Rbmps^{fl/fl}$ control mice (*SI Appendix*, Fig. S12*A*). We confirmed VSMC-specific *Rbpms* knockout in VSMCs isolated from $ApoE^{-/-}$;*Rbpms*-KO murine aortic root samples by magnetic bead selection (20) (*SI Appendix*, Fig. S12*B*). No significant differences in blood pressure, organ weights, peripheral blood cell counts, serum lipids, or serum cytokines were observed between $ApoE^{-/-}$;*Rbpms*-KO mice and controls at 16 wk of HFD (*SI Appendix*, Table S3). As with the *Rbpms*-overexpression model, we found statistically equivalent plaque formation levels and average plaque areas between $ApoE^{-/-}$;*Rbpms*-KO and controls (*SI Appendix*, Fig. S12 *C* and *D*). $ApoE^{-/-}$;*Rbpms*-KO plaques displayed enhanced cap/plaque and cap/core ratios (*SI Appendix*, Fig. S12 *E–G*), suggesting increased fibroproliferative VSMC activity in these plaques (19). $ApoE^{-/-}$;*Rbpms*-KO plaques displayed a smaller medial area (*SI Appendix*, Fig. S12*H*). These findings suggest that RBPMS reduces plaque cap development within atherosclerotic lesions in vivo.

RBPMS Reduces Postinjury Luminal Stenosis in *ApoE*$^{-/-}$ Mice. To explore the effects of RBPMS on luminal stenosis following vascular injury, we performed femoral cuff studies in *ApoE*$^{-/-}$;*Rbpms*-Tg and matching control *ApoE*$^{-/-}$;Ctrl-Tg mice. As expected, snap-frozen aortas from these mice were analyzed, and significant increases in *Rbpms* mRNA expression were observed in VSMC lineage (tdT+) cells from *ApoE*$^{-/-}$;*Rbpms*-Tg mice (*SI Appendix*, Fig. S13*A*). At 2 wk post–cuff placement, analyses were performed in neointimal lesion samples. Similar vessel surface areas were analyzed for cuffed portions of femoral arteries from *ApoE*$^{-/-}$;*Rbpms*-Tg and *ApoE*$^{-/-}$;Ctrl-Tg mice (*SI Appendix*, Fig. S13*B*). *ApoE*$^{-/-}$;*Rbpms*-Tg vessels revealed significant reductions in neointimal area (*SI Appendix*, Fig. S13*C*), intimal/medial ratio (*SI Appendix*, Fig. S13*D*), and luminal stenosis (*SI Appendix*, Fig. S13*E*). *ApoE*$^{-/-}$;*Rbpms*-Tg vessels also showed a lower VSMC (tdT+) cell percentage compared to controls (*SI Appendix*, Fig. S13*F*) but increased expression of the contractile VSMC marker ACTA2 (*SI Appendix*, Fig. S13*G*). We stained the vessels for the macrophage marker Mac3 and found no significant differences between *ApoE*$^{-/-}$;*Rbpms*-Tg and *ApoE*$^{-/-}$;Ctrl-Tg mice (*SI Appendix*, Fig. S13*H*).

We performed a similar study in *ApoE*$^{-/-}$;*Rbpms*-KO and matching control *ApoE*$^{-/-}$;*Rbmps*$^{fl/fl}$ mice. We confirmed VSMC-specific *Rbpms* knockout in VSMCs isolated from *ApoE*$^{-/-}$;*Rbpms*-KO murine aortic samples by magnetic bead selection (20) (*SI Appendix*, Fig. S14*A*). At 2 wk post–cuff placement, analyses were performed in neointimal lesion samples. Similar vessel surface areas were analyzed for cuffed portions of femoral arteries from *ApoE*$^{-/-}$;*Rbpms*-KO and control mice (*SI Appendix*, Fig. S14*B*). *ApoE*$^{-/-}$;*Rbpms*-KO vessels revealed significant increases in neointimal area (*SI Appendix*, Fig. S14*C*), intimal/medial ratio (*SI Appendix*, Fig. S14*D*), and luminal stenosis (*SI Appendix*, Fig. S14*E*). *ApoE*$^{-/-}$;*Rbpms*-KO vessels also showed a lower expression of the contractile VSMC marker ACTA2 (*SI Appendix*, Fig. S14*F*). Together, these data suggest that RBPMS reduces luminal stenosis post–vascular injury.

RBPMS Regulates the Expression and Alternative Splicing of the VSMC Master Regulator *MYOCD*. The transcriptional coactivator MYOCD, which interacts with regulatory CArG-box sequences located within the promoter and intronic regions of contractile apparatus genes, is regarded as a master regulator of VSMC differentiation (21). Given i) the positive link between *RBPMS* gene expression and VSMC contractile differentiation demonstrated here and ii) RBPMS's known role as a RNA-binding protein (11), we hypothesized that the RBPMS protein may regulate *MYOCD* mRNA expression in VSMCs. We collected harvested primary aortic VSMCs from *ApoE*$^{-/-}$;*Rbpms*-Tg mice and *ApoE*$^{-/-}$;Ctrl-Tg controls. Following a 7-d culture period, we found that *ApoE*$^{-/-}$;*Rbpms*-Tg VSMCs displayed significant increases in *Myocd* mRNA levels relative to *ApoE*$^{-/-}$;Ctrl-Tg VSMCs (Fig. 4*A*). Furthermore, HITC6 VSMCs in which RBPMS had been knocked down showed decreases in *MYOCD* mRNA levels relative to corresponding control VSMCs (Fig. 4*B*). We then explored the effects of RBPMS overexpression on *MYOCD* transcript levels by stably transducing HITA2 VSMCs with the RBPMS overexpression vector. RBPMS overexpression was sufficient to significantly increase *MYOCD* mRNA expression (Fig. 4*C*).

Distinct MYOCD protein isoforms, resulting from alternative splicing of the *MYOCD* pre-mRNA (Fig. 4*D*), show differing impacts on the contractile differentiation of VSMCs (10). Specifically, *MYOCD_v3* variants (i.e., the v3a variant including exon 2a and the v3b variant with deletion of the first two exons) produce strong contractile activity and low proliferative activity in vitro. In contrast, *MYOCD_v1* variants (i.e., the v1a variant lacking exon 2a and the v1b variant lacking exon 2a as well as ATG2 and ATG3) produce low contractile activity and moderate proliferative activity in vitro. The RBPMS protein, by promoting inclusion of exon 2a within the mature *MYOCD* mRNA, results in a premature stop codon and generates the 856-amino acid *MYOCD_v3a* variant that more potently supports the contractile VSMC phenotype (11, 22). Based on this evidence, we hypothesized that RBPMS may influence the alternative splicing of the *MYOCD* pre-mRNA in favor of the procontractile *MYOCD_v3a* variant.

We explored the ability of RBPMS to bind to the *MYOCD* pre-mRNA through RIP assays using an anti-RBPMS antibody in HITA2 VSMC lysates. We confirmed binding between RBPMS and the *MYOCD* pre-mRNA that was significantly stronger in HITA2 VSMCs with RBPMS overexpression (Fig. 4*E*). We then evaluated the link between RBPMS overexpression and *MYOCD* alternative splicing by analyzing *MYOCD_v3a* and *MYOCD_v1a/b* levels in murine and human VSMCs (Fig. 4*F*). Following serial passaging, exclusive *Myocd_v1a/b* expression was observed in VSMCs from *ApoE*$^{-/-}$;Ctrl-Tg mice, while significantly greater *Myocd_v3a* was detected in *ApoE*$^{-/-}$;*Rbpms*-Tg VSMCs (Fig. 4*G*). This was confirmed by enhanced *MYOCD_v3a* in HITA2 VSMCs following RBPMS overexpression (Fig. 4*H*). To further confirm this relationship between RBPMS and *MYOCD_v3a* upregulation, we collected RNA from HITC6 VSMCs that had been cultured in FCS-containing media (FCS+, day 0) and from these same cells following eight days of serum starvation (FCS–, day 8), which induces a contractile phenotype. On day 0, *MYOCD_v1a/b* expression was predominant in proliferative shCtrl-transduced HITC6 VSMCs, whereas *MYOCD_v3a* was less abundant in shRBPMS-transduced HITC6 VSMCs (Fig. 4*I*). On day 8, serum starvation enhanced RBPMS and *MYOCD_v3a* expression in shCtrl VSMCs, which were both abrogated by shRBPMS. As MYOCD_v1a's anti-contractile effects are mediated through its interaction with the transcription factor myocyte enhancing factor 2 (MEF2) (23), we analyzed expression levels of the four MEF2 isoforms (MEF2A-D) in HITC6 VSMCs. On day 0, MEF2A, MEF2B, and MEF2D expression were observable in proliferative shCtrl-transduced HITC6 VSMCs (*SI Appendix*, Fig. S15). On day 8, serum starvation reduced MEF2A expression but did not affect the other isoforms in shCtrl VSMCs. Notably, RBPMS knockdown had no significant impact on any of the MEF2 isoforms.

To evaluate RBPMS's function as a direct regulator of *MYOCD* exon 2a alternative splicing, we employed Van Der Veer et al.'s *MYOCD* exon 2a minigene construct in HEK293T cells (*SI Appendix*, *Methods* and ref. 10). RBPMS binds to RNAs through tandem CAC motifs within intronic regions adjacent to target exons (11, 24, 25). We focused on two proven RBPMS binding sequences, CAC1 and CAC2, adjacent to exon 2a on the *MYOCD* pre-mRNA (*SI Appendix*, Fig. S16 and ref. 11). Mutation of both CAC1 and CAC2 abolishes RBPMS's ability to splice the *MYOCD* strand (11). Two *MYOCD* exon 2a minigene constructs were prepared: one containing the WT *MYOCD* exon 2a coding sequence and WT CAC1 and CAC2 sequences (WT-2a-CAC1/2), and the other containing the WT *MYOCD* exon 2a coding sequence and mutated CAC1 and CAC2 sequences (MUT-2a-CAC1/2). The MUT-2a-CAC1/2 construct was associated with a significant decrease in exon 2a incorporation into the final *MYOCD* transcript relative to the WT-2a-CAC1/2 construct (Fig. 4*J*). WT RBPMS overexpression enhanced exon 2a incorporation, while overexpression of the RBPMS RNA recognition motif (RRM) mutant RBPMS$^{F65A/K100E}$ (24) did not significantly impact exon 2a incorporation (Fig. 4*J* and *SI Appendix*, Fig. S17). This evidence indicates that RBPMS's RRM RNA-binding domain and the *MYOCD* WT CAC1/2 motifs are necessary for exon 2a incorporation into the *MYOCD* transcript.

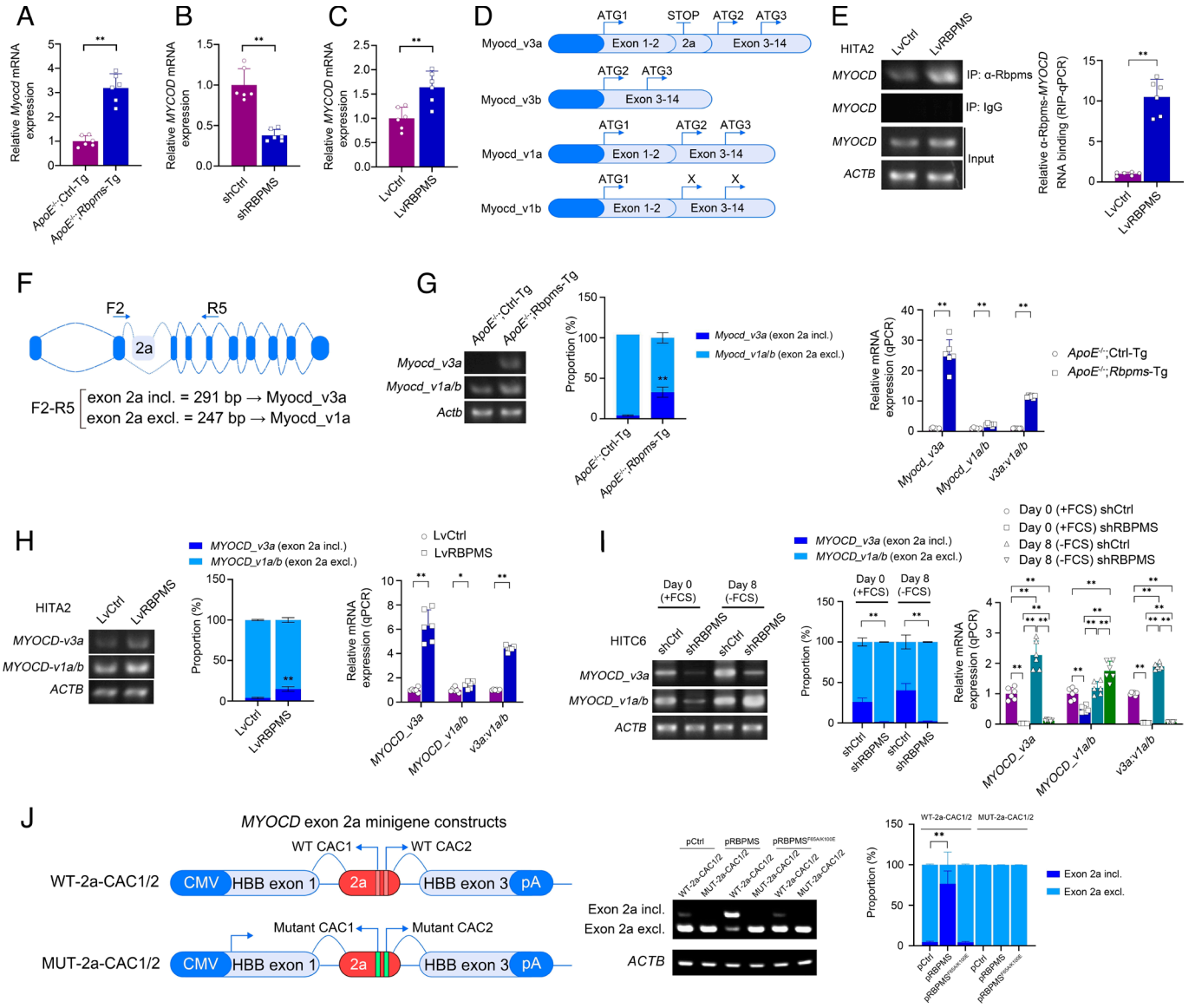

Fig. 4. RBPMS regulates the expression and alternative splicing of the VSMC master regulator *MYOCD*. (*A*) Relative *Myocd* mRNA expression levels in aortic VSMCs derived from *ApoE*$^{-/-}$;*Rbpms*-Tg and *ApoE*$^{-/-}$;Ctrl-Tg mice. (*B* and *C*) Relative *MYOCD* mRNA expression levels in (*B*) HITC6 VSMCs transduced with RBPMS shRNA (shRBPMS) or control shRNA (shCtrl) and (*C*) HITA2 VSMCs following *RBPMS* cDNA overexpression vector (LvRBPMS) or control overexpression vector (LvCtrl) transduction. (*D*) Schematic illustrating the four primary *Myocd* isoforms in VSMCs. Please note the primary start codon (ATG1), the two alternative start codons (ATG2, ATG3), and a premature stop codon within exon 2a. (*E*) Goat anti-rabbit RBPMS antibody or a control goat anti-rabbit IgG antibody was used for *Myocd* RNA immunoprecipitation (RIP, *Right*) and RIP-qPCR (*Left*). (*F*) Schematic overview of the RT-PCR primers used to evaluate *Myocd_v3a* and *Myocd_v1a/b* splice variants in panels *G*–*I*. The alternatively spliced *Myocd* exon 2a is indicated with the light gray box, with RT-PCR quantification being based upon the proportions (%) of exon 2a inclusion and exclusion. (*G*) *Myocd_v3a* and *Myocd_v1a/b* expression within *ApoE*$^{-/-}$;*Rbpms*-Tg and *ApoE*$^{-/-}$;Ctrl-Tg VSMCs were assessed via RT-PCR (*Right*) and qPCR (*Left*). (*H*) Following *RBPMS* cDNA overexpression vector (LvRBPMS) or control overexpression vector (LvCtrl) transduction of HITA2 VSMCs, RT-PCR (*Right*) and qPCR (*Left*) were used to analyze *MYOCD_v3a* and *MYOCD_v1a/b* expression. (*I*) Following stable ShRBPMS or shCtrl transduction of HITC6 VSMCs and culture with serum (+FCS, day 0) or on day 8 following serum removal (−FCS), these cells were analyzed via RT-PCR and qPCR to assess *MYOCD_v3a* and *MYOCD_v1a/b* expression. (*J*) Overview of pDup-2a splicing reporters designed based upon the *Myocd* exon 2a sequence (red), which was inserted into the pDup51 vector that codes for human β-globin (*HBB*) exons 1 and 3. The WT RBPMS binding sites CAC1/2 in exon 2a (pink) were mutated (green) as detailed in the *Materials and Methods*. RNA from HEK293T cells was harvested at 24 h posttransfection with the indicated constructs and was analyzed via RT-PCR. $n = 6$ biological replicates/group for all experiments. Data represented as means ± SDs. *$P < 0.05$, **$P < 0.01$ [(*A*–*C*, *E*, *G*, and *H*) unpaired two-tailed *t*-test; (*I* and *J*) two-way ANOVA].

In sum, RBPMS enhances *MYOCD* exon 2a inclusion and resultant procontractile *MYOCD_v3a* expression with no significant impact on MEF2 levels.

RBPMS Promotes Contractile Differentiation and Reduces Fibroproliferative Activity of VSMCs Through MYOCD_v3a Upregulation. To better understand the impact of RBPMS's regulation of *MYOCD* alternative splicing on the VSMC phenotype, we collected *ApoE*$^{-/-}$;*Rbpms*-Tg and *ApoE*$^{-/-}$;Ctrl-Tg primary aortic VSMCs and subjected them to *Myocd_v3a* siRNA (siMyocd_v3a) or control siRNA (siCtrl) transfection (*SI Appendix*, Fig. S18*A*). *ApoE*$^{-/-}$;*Rbpms*-Tg VSMCs exhibited reductions in proliferative activity (Fig. 5*A*), collagen production (Fig. 5*B*), and migratory activity in a Transwell assay (Fig. 5*C*), which were all rescued by *Myocd_v3a* knockdown. *ApoE*$^{-/-}$;*Rbpms*-Tg VSMCs exhibited significant increases in the expression of the contractile apparatus genes, which was abrogated by *Myocd_v3a* knockdown (Fig. 5*D*). Western blotting further confirmed an increase in ACTA2 protein levels in *ApoE*$^{-/-}$;*Rbpms*-Tg VSMCs, which was abrogated by *Myocd_v3a* knockdown (Fig. 5*E*).

We subjected HITC6 VSMCs to lentiviral *RBPMS* shRNA (shRBPMS+LvCtrl), lentiviral *RBPMS* shRNA plus *MYOCD_v3a*

overexpression (shRBPMS+LvMYOCD_v3a), or control vector (shCtrl+LvCtrl) transduction (*SI Appendix*, Fig. S18*B*). *RBPMS* knockdown in HITC6 VSMCs resulted in increased proliferation (Fig. 5*F*), collagen synthesis (Fig. 5*G*), and migration (Fig. 5*H*), which were all abrogated by *MYOCD_v3a* overexpression. We observed significant decreases in mRNA and protein levels of contractile apparatus components following *RBPMS* knockdown, which were rescued by *MYOCD_v3a* overexpression (Fig. 5 *I* and *J*).

We next subjected HITA2 VSMCs to lentiviral *RBPMS* overexpression (LvRBPMS+shCtrl), lentiviral *RBPMS* overexpression plus *MYOCD_v3a* knockdown (LvRBPMS+shMYOCD_v3a), or control vector (LvCtrl+shCtrl) transduction (*SI Appendix*, Fig. S18*C*). *RBPMS* overexpression in HITA2 VSMCs increased mRNA and protein levels of contractile apparatus components, which was abrogated by *MYOCD_v3a* knockdown (Fig. 5 *K* and *L*). We additionally evaluated the effects of *RBPMS* overexpression on contractile activity by plating lentivirally transfected HITA2 VSMCs onto a silicone elastomer substrate that can be deformed in response to cellular contractile activity, as evidenced by visible wrinkles when assessed via phase-contrast microscopy. Control HITA2 VSMCs were not able to deform this substrate. A majority of *RBPMS*-overexpressing VSMCs functionally contracted the elastomer substrate, which was abrogated by *MYOCD_v3a* knockdown (Fig. 5*M*). Together, these data provide strong evidence that RBPMS drives VSMCs toward a more contractile phenotype and reduces their fibroproliferative activity through *MYOCD_v3a* upregulation.

RBPMS Promotes Procontractile *Myocd_v3a* Skewing in VSMCs Within Atherosclerotic and Postinjury Arteries. To establish whether RBPMS regulates *Myocd* alternative splicing in atherosclerotic VSMCs in vivo, we employed our afore-described HFD-fed *ApoE*$^{-/-}$;*Rbpms*-Tg and *ApoE*$^{-/-}$;Ctrl-Tg mice. Atherosclerotic aortic roots were analyzed after 16 wk of HFD in order to assess the effects of VSMC-specific *Rbpms* overexpression. As expected, *ApoE*$^{-/-}$;*Rbpms*-Tg mice displayed significantly enhanced *Rbpms* and *Myocd* expression levels in VSMC lineage (tdT+) cells relative to *ApoE*$^{-/-}$;Ctrl-Tg controls following 16 wk of HFD (*SI Appendix*, Fig. S19*A*). Moreover, *ApoE*$^{-/-}$;*Rbpms*-Tg mice displayed enhanced *Myocd_v3a* expression in VSMC lineage (tdT+) cells following 16 wk of HFD (*SI Appendix*, Fig. S19*B*).

To establish whether RBPMS regulates *Myocd* splicing following acute vascular injury, we employed the afore-described femoral cuff model in HFD-fed *ApoE*$^{-/-}$;Ctrl-Tg and *ApoE*$^{-/-}$;*Rbpms*-Tg mice. On day 0 (prior to injury) and on days 1, 3, 5, 7, and 14 d postinjury, vessel samples were collected and *Rbpms*, total *Myocd*, *Myocd_v3a*, and *Myocd_v1a/b* transcript levels in VSMC lineage (tdT+) cells therein were assessed. Vessel injury in *ApoE*$^{-/-}$;Ctrl-Tg controls led to a decrease in *Rbpms* and *Myocd* expression levels in VSMC lineage (tdT+) cells, which was reversed in *ApoE*$^{-/-}$;*Rbpms*-Tg mice (*SI Appendix*, Fig. S19*C*). *Myocd_v3a* and *Myocd_v1a/b* transcript coexpression was observed through day 14 postinjury. *Myocd_v3a* expression was lower on days 3-14 in *ApoE*$^{-/-}$;Ctrl-Tg controls, which was reversed in *ApoE*$^{-/-}$;*Rbpms*-Tg mice (*SI Appendix*, Fig. S19*D*). These results support a model wherein RBPMS's alternative splicing of the *Myocd* pre-mRNA occurs under physiologically relevant conditions, leading to *Myocd_v3a* skewing that promotes a contractile VSMC phenotype within the injured arterial wall.

Discussion

This work highlights the key role that the RNA-binding protein RBPMS plays in inhibiting VSMC modulation and maintaining VSMC differentiation within the diseased vessel wall. Our initial scRNAseq analysis identified *RBPMS* as a conserved, VSMC-specific gene positively associated with contractile VSMC differentiation in atherosclerosis. Our follow-up studies revealed significant *RBPMS* gene downregulation in both atherosclerotic and injured vessel VSMCs, leading us to hypothesize that RBPMS may inhibit VSMC modulation and thereby reduce VSMC-driven plaque cap development and intervention-induced restenosis. To explore this question in vivo, we generated transgenic mouse lines exhibiting VSMC-specific *Rbpms* overexpression or VSMC-specific *Rbpms* knockout. In our atherosclerosis models, *Rbpms* suppressed fibrous cap development, overall plaque VSMC content, and fibrous cap VSMC content while enhancing vessel expression of the contractile VSMC marker ACTA2. Consistently, in our vascular injury model, *Rbpms* reduced neointimal formation, luminal stenosis, and vessel VSMC content while enhancing vessel expression of ACTA2. Fate mapping studies in murine aortic root lesions suggest that modulated VSMCs climb from the medial layer at 6 wk of HFD feeding to form and grow the fibrous cap and then return down to the plaque's interior where they contribute to plaque growth (26). In contrast, contractile VSMCs do not display these migratory, fibroproliferative characteristics. Therefore, *Rbpms* appears to promote a differentiated, contractile VSMC phenotype while blocking the modulated VSMC transcriptional program that drives hyperproliferation, migration, and ECM deposition in the diseased vessel wall. This evidence suggests that RBPMS may play a role in inhibiting VSMC-driven plaque cap development and intervention-induced restenosis. It should be noted that plaque cap rupture, which exposes the thrombogenic, lipid-rich plaque core to platelets and red blood cells, is the primary cause of thromboembolic events from coronary and carotid atherosclerosis (27). Reduced cap/plaque and cap/core ratios are indicators of plaque cap vulnerability to rupture (19). *ApoE*$^{-/-}$;*Rbpms*-Tg plaques displayed reduced cap/plaque and cap/core ratios, while *ApoE*$^{-/-}$;*Rbpms*-KO plaques displayed enhanced cap/plaque and cap/core ratios. RBPMS, by inhibiting VSMC-driven plaque cap development, may contribute to plaque cap vulnerability.

There are several core transcription factors that govern VSMC differentiation [extensively reviewed here (28)]. Most notably, the transcription factor SRF and its transcriptional coactivator MYOCD act on the CArG-box regulatory sequences located in the promoter and intronic regions of contractile genes, including *ACTA2*, *CNN1*, and *MYH11* (21). Thus, the SRF-MYOCD complex plays a critical role in promoting VSMC contractile differentiation (21) and supports procontractile *RBPMS* gene expression in VSMCs (18). Here, we show that PDGF-BB, through its receptor PDGFRβ, downregulates *RBPMS* gene expression through promoting ELK1^{S383} phosphorylation, which displaces MYOCD from the SRF-MYOCD complex. Our findings are consistent with previous studies showing vascular injury-induced PDGF-BB upregulates p-ELK1^{S383}, which competitively displaces MYOCD from the SRF-MYOCD complex to form the SRF-p-ELK1^{S383} complex (16, 17).

Two distinct MYOCD protein isoforms, MYOCD_v1a and MYOCD_v3a, result from alternative splicing of the *MYOCD* pre-mRNA (29). MYOCD_v3a (which includes exon 2a) is the dominantly expressed MYOCD variant in healthy VSMCs; VSMCs expressing comparable *MYOCD_v1a* and *MYOCD_v3a* transcript levels display substantially higher MYOCD_v3a protein levels (10). Both MYOCD_v1a and MYOCD_v3a function as transcriptional coactivators for SRF (29). However, MYOCD_v1a and MYOCD_v3a show differing impacts on the contractile differentiation of VSMCs (10). MYOCD_v1a alone possesses an N-terminal region that enables it to interact with MEF2 (23). This MEF2-MYOCD_v1a interaction antagonistically competes

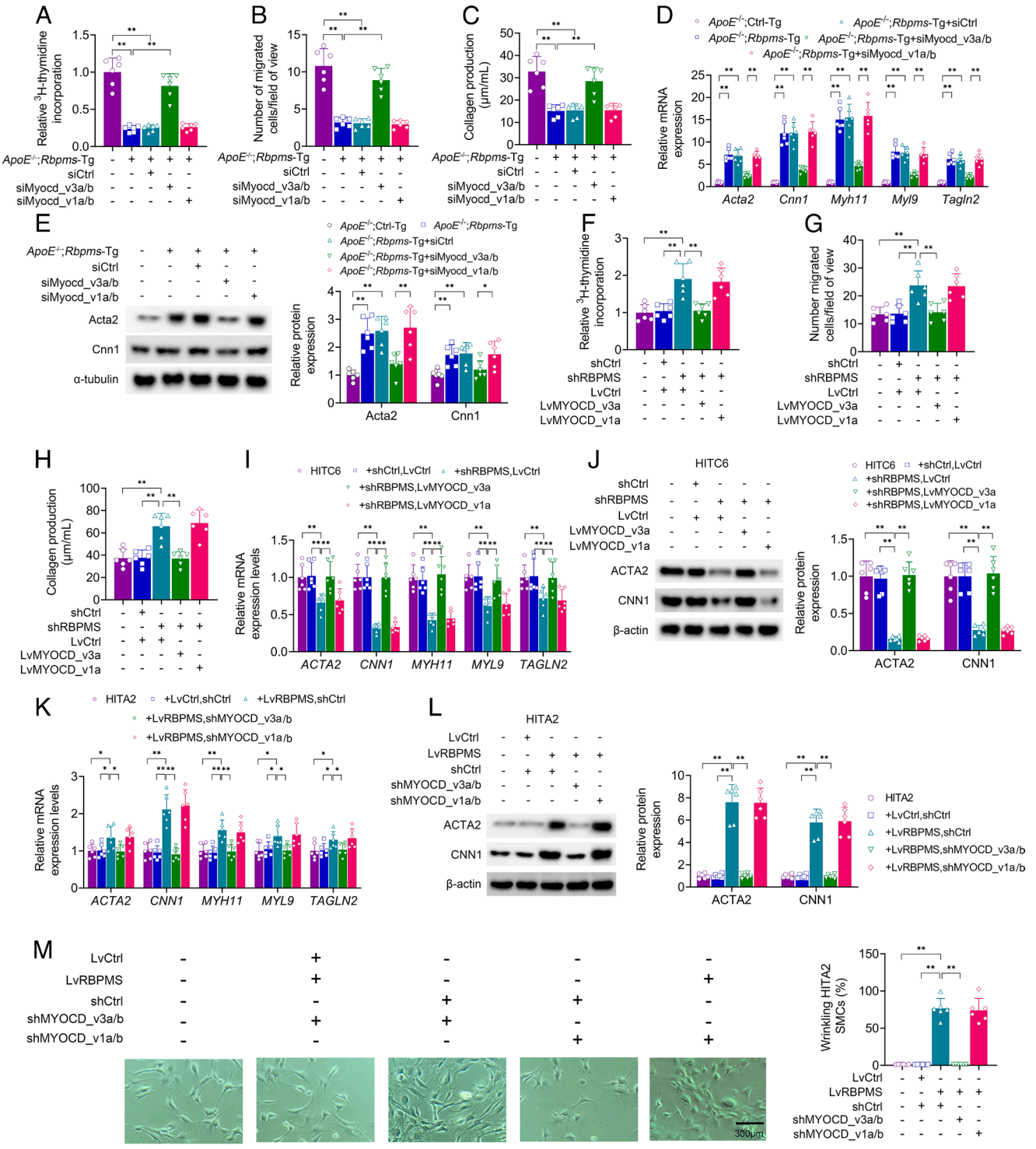

Fig. 5. RBPMS promotes contractile differentiation and reduces fibroproliferative activity of VSMCs through MYOCD_v3a upregulation. (*A–E*) Aortic VSMCs were isolated from *ApoE*$^{-/-}$;*Rbpms*-Tg and *ApoE*$^{-/-}$;Ctrl-Tg mice and transduced with Myocd_v3a siRNA (siMyocd_v3a) or control siRNA (siCtrl). (*A*) [3H]-thymidine uptake was used to quantify VSMC proliferation in disintegrations per minute (dpm). (*B*) VSMC migration in the presence of a formyl methionyl leucyl phenylalanine (fMLP) gradient was tested in a Transwell assay (10 fields of view per well). (*C*) The collagen-producing activity of VSMCs was quantified. (*D*) Levels of contractile apparatus-related gene expression were assessed in VSMCs. *Actb* was used as a housekeeping control. (*E*) Smooth muscle α-actin levels in aortic explant cultures from *ApoE*$^{-/-}$;*Rbpms*-Tg and *ApoE*$^{-/-}$;Ctrl-Tg controls were measured via western blotting. α-tubulin was used for normalization. (*F–J*) HITC6 VSMCs were transduced with RBPMS shRNA (shRBPMS) or control shRNA (shCtrl) without or with rescue *MYOCD_v3a* cDNA (LvMYOCD_v3a) overexpression. (*F*) Proliferation was assessed by measuring [3H]-thymidine uptake (dpm), (*G*) VSMC migration in the presence of a fMLP gradient was tested in a Transwell assay (10 fields of view per well), and (*H*) collagen production activity was measured. (*I*) Levels of contractile apparatus-related gene expression were assessed in VSMCs. *ACTB* was used as a housekeeping control. (*J*) Contractile apparatus-related protein expression was assessed via western blotting. (*K–M*) HITA2 VSMCs were transduced with *RBPMS* cDNA overexpression vector (LvRBPMS) or control overexpression vector (LvCtrl) without or with rescue MYOCD_v3a shRNA (shMYOCD_v3a). (*K*) Levels of contractile apparatus-related gene expression were assessed in VSMCs. *ACTB* was used as a housekeeping control. (*L*) Contractile apparatus-related protein expression was assessed via western blotting. (*M*) HITA2 VSMCs plated on a deformable elastomer substrate (5 kPa) following lentiviral transduction were imaged, and the frequencies of contraction-competency among these cells were quantified. (Scale bar, 300 μm.) $n = 6$ biological replicates/group for all experiments. Data represented as means ± SDs. *$P < 0.05$, **$P < 0.01$ [(*A–M*) one-way ANOVA].

with the procontractile SRF-MYOCD_v1a interaction, as MEF2 dose-dependently titrates MYOCD_v1a away from SRF (23).

Here, we found that RBPMS functions as an important post-transcriptional *MYOCD* pre-mRNA regulator in VSMCs by favoring *MYOCD_v3a* over *MYOCD_v1a* with no significant impact on MEF2 levels. This is in direct contrast to another RNA-binding protein Quaking (Qkl), which favors *MYOCD_v1a* over the *MYOCD_v3a* (10). Indeed, Nakagaki-Silva et al.'s in vitro work suggests that RBPMS and Qkl opposingly regulate *MYOCD* exon 2a inclusion through antagonistic, competitive binding on the *MYOCD* pre-mRNA (11). The strong RBPMS expression and weak Qkl expression within healthy arterial wall VSMCs that exhibit the near-exclusive *MYOCD_v3a* expression coupled with weak RBPMS expression and strong Qkl expression within diseased arterial wall VSMCs that exhibit significantly lower *MYOCD_v3a* provides further support for the physiological relevance of RBPMS and Qkl as key opposing regulators of *MYOCD* pre-mRNA alternative splicing in arterial wall VSMCs (10). We postulate that RBPMS downregulation and Qkl upregulation in atherosclerotic and injured vessel VSMCs, which enhances MYOCD_v1a skewing and resultant MEF2-MYOCD_v1a interactivity, shifts VSMCs away from the procontractile SRF transcriptional program toward a fibroproliferative phenotype. Therefore, promoting RBPMS activity and/or inhibiting Qkl activity in diseased vascular wall VSMCs should enhance MYOCD_v3a skewing to support the procontractile SRF transcriptional program. Further mechanistic research on the precise relationships between RBPMS, Qkl, MYOCD_v3a, MYOCD_v1a, and MEF2-MYOCD_v1a interactivity and their effects on the SRF transcriptional program and contractile phenotype in VSMCs will be needed to validate this model.

In addition to *MYOCD*, RBPMS may regulate the expression or splicing of other pre-mRNAs associated with VSMC modulation. Based on studies in neonatal rat ventricular cardiomyocytes, RBPMS interacts with several members of the splicing-related heterogeneous nuclear ribonucleoprotein (hnRNP) protein family and regulates the splicing of multiple sarcomere-associated pre-mRNAs (e.g., *Pdlim5*, *Nexn*, and *Ttn*) (24). In addition, RBPMS may regulate RNA-associated processes other than pre-mRNA splicing. Previous work reveals that RBPMS localizes to cytoplasmic stress granules in HEK293 cells (30) and cytoplasmic RNP granules in RGC-5 retinal cells (31), suggesting RBPMS's involvement in mRNA transport. Therefore, further research on RBPMS's function in VSMC modulation is warranted.

In conclusion, the RNA-binding protein RBPMS inhibits VSMC modulation and maintains VSMCs in a differentiated, contractile state by regulating the expression and alternative pre-mRNA splicing of the VSMC master regulator *MYOCD*. This evidence suggests that RBPMS may play a role in inhibiting VSMC-driven plaque cap development and intervention-induced restenosis.

Materials and Methods

Ethics Statement. The Ethics Committee of the First People's Hospital of Yunnan approved all human patient protocols for this study (approval no. KHLL2024-KY220). Written informed consent was obtained from all patients prior to enrollment. The Animal Care and Use Committee of Chongqing Medical University approved all animal protocols for this study (approval no. 2022734). All animal procedures were conducted in accordance with the NIH Guide for the Care and Use of Laboratory Animals (Bethesda, MD). Animals were raised with ad libitum normal chow and water access in a temperature-controlled facility (26 °C) with a 12 h light/dark cycle (7 AM to 7 PM). The animals were humanely killed via cervical dislocation under deep anesthesia.

scRNAseq Data Analysis. The murine scRNAseq data from the HFD-fed atherosclerotic mouse model (GEO acc. no.: GSE131776) and human scRNAseq data from dissociated right coronary artery cells (GEO acc. no.: GSE131778) are available from the GEO database. For detailed procedures, see *SI Appendix, Methods*.

Human Carotid Atheroma Study. See *SI Appendix, Methods*.

Transcriptomics Analysis in Rat VSMCs. See *SI Appendix, Methods*.

VSMC Culture and RBPMS Modulation. For primary aortic murine VSMC isolation, DMEM supplemented with 10% FCS and 0.01 μg/mL glutamine were used to culture murine aortic explants under standard incubation (37 °C, 5% CO_2). The human internal thoracic VSMC clonal lines (HITC6 and HITA2) were generated as previously described (32). VSMCs were grown under proliferative or differentiating culture conditions as previously described by Llorian et al. (33). Details regarding RBPMS modulation in cultured VSMCs are provided in *SI Appendix, Methods*.

qPCR. Oligo-dT primers (Invitrogen) were utilized for cDNA preparation other than in immunoprecipitation and alternative transcript experiments, in which case random primers (Invitrogen) were used to prepare cDNA. All qPCR analyses were performed with SYBR Green master mix (Bio-Rad) together with the primers detailed in *SI Appendix*, Table S4. Either *ACTB* or *Actb* was used as the housekeeping control.

Coimmunoprecipitation (co-IP), Western Blotting, and ELISA. Conventional co-IP, SDS-PAGE, and immunoblotting protocols were used to isolate, separate, and stain proteins (34). For co-IP, rabbit anti-SRF antibodies were coupled to anti-rabbit IgG-conjugated magnetic beads (#11-203-D, Dynabeads M-280 Sheep Anti-Rabbit IgG, Invitrogen). Either α-tubulin or β-actin was used as the loading control. All primary and secondary antibodies are detailed in *SI Appendix*, Table S5. ELISA kits for human p-ELK1^{S383} (#abx596610) and human RBPMS (#abx382742) were purchased from Abbexa.

Animal Models. See *SI Appendix, Methods* for the construction of *ApoE*$^{-/-}$ transgenic mice. Detailed procedures regarding the murine atherosclerosis model, the rat carotid injury model, and the murine femoral cuff model are also provided in *SI Appendix, Methods*.

In Vitro VSMC Assays. Please see *SI Appendix, Methods* for detailed procedures regarding in vitro VSMC assays, including proliferation, migration, collagen production, contractility, and RIP for RBPMS-*MYOCD* pre-mRNA binding.

***MYOCD* exon 2a Minigene Construct.** Please see *SI Appendix, Methods*.

Statistical Analysis. All animal experiments were conducted using a simple randomization approach using coding to enable blinded analyses. All samples that were available were analyzed for individual experiments, without any exclusion of specific animals. GraphPad Prism 6 and Bioconductor were used for all statistical testing. The Shapiro–Wilks test was used to determine whether data conformed to a normal distribution. Samples were compared using two-tailed *t* tests or Mann–Whitney *U* tests for pairwise comparisons. Multiple comparisons were made via one-way ANOVAs or Kruskal–Wallis tests with Bonferroni or Dunn's multiple comparison test for parametric and nonparametric data, respectively. $P < 0.05$ served as the significance threshold for all analyses.

Data, Materials, and Software Availability. All study data are included in the article and/or supporting information. The code for the bioinformatics analyses are available upon request.

ACKNOWLEDGMENTS. We would like to thank Dr. Hector Hernandez-Vargas (Genomics Consulting, 69500 Bron, France) for his technical assistance with the bioinformatics pipeline and associated analyses. This work was supported by the National Natural Science Foundation of China (81960095 and 81871369). The funders had no role in study design, data collection and analysis, decision to publish, or preparation of the manuscript.

Author affiliations: [a]Department of Ultrasound, The Second Affiliated Hospital of Chongqing Medical University, Chongqing 400016, China; [b]Department of Nephrology, The Second Affiliated Hospital of Chongqing Medical University, Chongqing 400016, China; [c]Precision Medicine Center, The Second Affiliated Hospital of Chongqing Medical University, Chongqing Municipality Clinical Research Center for Geriatrics and Gerontology, Chongqing 400016, China; [d]Department of Cardiology, The Second Affiliated Hospital of Chongqing Medical University, Chongqing 400016, China; [e]Chongqing Key Laboratory of Ultrasound Molecular Imaging and Therapy, Chongqing 400016, China; [f]Department of Rehabilitation and Pain Medicine, The Ninth People's Hospital of Chongqing, Chongqing 400700, China; [g]Impactys Foundation for Biomedical Research, San Diego, CA 92121; [h]Department of Cardiothoracic Surgery, The First People's Hospital of Yunnan Province, The Affiliated Hospital of Kunming University of Science and Technology, Kunming 363880, China; [i]Center for Translational Research in Clinical Medicine, School of Medicine, Kunming University of Science and Technology, Kunming 650500, China; and [j]Department of Cardiothoracic Surgery, The Affiliated Hospital of Kunming University of Science and Technology, Kunming 363880, China

1. W. C. Zheng, W. Chan, A. Dart, J. A. Shaw, Novel therapeutic targets and emerging treatments for atherosclerotic cardiovascular disease. *Eur. Heart J. Cardiovasc. Pharmacother.* **10**, 53–67 (2024).
2. R. C. Wirka *et al.*, Atheroprotective roles of smooth muscle cell phenotypic modulation and the TCF21 disease gene as revealed by single-cell analysis. *Nat. Med.* **25**, 1280–1289 (2019).
3. J. W. Jukema, J. J. Verschuren, T. A. Ahmed, P. H. Quax, Restenosis after PCI. Part 1: Pathophysiology and risk factors. *Nat. Rev. Cardiol.* **9**, 53–62 (2012).
4. J. W. Jukema, T. A. Ahmed, J. J. Verschuren, P. H. Quax, Restenosis after PCI. Part 2: Prevention and therapy. *Nat. Rev. Cardiol.* **9**, 79–90 (2012).
5. M. Liu, D. Gomez, Smooth muscle cell phenotypic diversity: At the crossroads of lineage tracing and single-cell transcriptomics. *Arterioscler. Thromb. Vasc. Biol.* **39**, 1715–1723 (2019).
6. J. Aoki, K. Tanabe, Mechanisms of drug-eluting stent restenosis. *Cardiovasc. Interv. Ther.* **36**, 23–29 (2021).
7. L. S. Shankman *et al.*, KLF4-dependent phenotypic modulation of smooth muscle cells has a key role in atherosclerotic plaque pathogenesis. *Nat. Med.* **21**, 628–637 (2015).
8. J.-D. Lin *et al.*, Single-cell analysis of fate-mapped macrophages reveals heterogeneity, including stem-like properties, during atherosclerosis progression and regression. *JCI Insight* **4**, e124574 (2019).
9. I. Toma, T. A. McCaffrey, Transforming growth factor-β and atherosclerosis: Interwoven atherogenic and atheroprotective aspects. *Cell Tissue Res.* **347**, 155–175 (2012).
10. E. P. van der Veer *et al.*, Quaking, an RNA-binding protein, is a critical regulator of vascular smooth muscle cell phenotype. *Circ. Res.* **113**, 1065–1075 (2013).
11. E. E. Nakagaki-Silva *et al.*, Identification of RBPMS as a mammalian smooth muscle master splicing regulator via proximity of its gene with super-enhancers. *Elife* **8**, e46327 (2019).
12. A. C. van Dijk *et al.*, Intraplaque hemorrhage and the plaque surface in carotid atherosclerosis: The Plaque at RISK Study (PARISK). *Am. J. Neuroradiol.* **36**, 2127–2133 (2015).
13. L. Schnack *et al.*, Mechanisms of trained innate immunity in oxLDL primed human coronary smooth muscle cells. *Front. Immunol.* **10**, 13 (2019).
14. U. Rykaczewska *et al.*, PCSK6 is a key protease in the control of smooth muscle cell function in vascular remodeling. *Circ. Res.* **126**, 571–585 (2020).
15. J. Zhou, L. Shao, J. Yu, J. Huang, Q. Feng, PDGF-BB promotes vascular smooth muscle cell migration by enhancing Pim-1 expression via inhibiting miR-214. *Ann. Transl. Med.* **9**, 1728 (2021).
16. Y. Xu *et al.*, SRF SUMOylation modulates smooth muscle phenotypic switch and vascular remodeling. *Nat. Commun.* **15**, 6919 (2024).
17. F. Gualdrini *et al.*, SRF co-factors control the balance between cell proliferation and contractility. *Mol. Cell* **64**, 1048–1061 (2016).
18. L. Liu *et al.*, Myocardin regulates exon usage in smooth muscle cells through induction of splicing regulatory factors. *Cell. Mol. Life Sci.* **79**, 459 (2022).
19. M. O. Grootaert, A. Finigan, N. L. Figg, A. K. Uryga, M. R. Bennett, SIRT6 protects smooth muscle cells from senescence and reduces atherosclerosis. *Circ. Res.* **128**, 474–491 (2021).
20. J. Chen *et al.*, Isolation and culture of murine aortic cells and RNA isolation of aortic intima and media: Rapid and optimized approaches for atherosclerosis research. *Atherosclerosis* **347**, 39–46 (2022).
21. L. M. Khachigian *et al.*, Transcriptional regulation of vascular smooth muscle cell proliferation, differentiation and senescence: Novel targets for therapy. *Vasc. Pharmacol.* **146**, 107091 (2022).
22. M. Imamura, X. Long, V. Nanda, J. M. Miano, Expression and functional activity of four myocardin isoforms. *Gene* **464**, 1–10 (2010).
23. E. E. Creemers, L. B. Sutherland, J. Oh, A. C. Barbosa, E. N. Olson, Coactivation of MEF2 by the SAP domain proteins myocardin and MASTR. *Mol. Cell* **23**, 83–93 (2006).
24. P. Gan *et al.*, RBPMS regulates cardiomyocyte contraction and cardiac function through RNA alternative splicing. *Cardiovasc. Res.* **120**, 56–68 (2024).
25. M. Teplova, T. A. Farazi, T. Tuschl, D. J. Patel, Structural basis underlying CAC RNA recognition by the RRM domain of dimeric RNA-binding protein RBPMS. *Q. Rev. Biophys.* **49**, e1 (2016).
26. A. Misra *et al.*, Integrin beta3 regulates clonality and fate of smooth muscle-derived atherosclerotic plaque cells. *Nat. Commun.* **9**, 1–13 (2018).
27. D. G. Jovin, B. E. Sumpio, D. M. Greif, Manifestations of human atherosclerosis across vascular beds. *JVS-Vasc. Insights* **2**, 100089 (2024).
28. Y. Jiang, H.-Y. Qian, Transcription factors: Key regulatory targets of vascular smooth muscle cell in atherosclerosis. *Mol. Med.* **29**, 2 (2023).
29. S. Sahoo *et al.*, MEF2C-MYOCD and leiomodin1 suppression by miRNA-214 promotes smooth muscle cell phenotype switching in pulmonary arterial hypertension. *PLoS One* **11**, e0153780 (2016).
30. T. A. Farazi *et al.*, Identification of the RNA recognition element of the RBPMS family of RNA-binding proteins and their transcriptome-wide mRNA targets. *RNA* **20**, 1090–1102 (2014).
31. M. T. Furukawa, H. Sakamoto, K. Inoue, Interaction and colocalization of HERMES/RBPMS with NonO, PSF, and G3 BP 1 in neuronal cytoplasmic RNP granules in mouse retinal line cells. *Genes Cells* **20**, 257–266 (2015).
32. S. Li *et al.*, Innate diversity of adult human arterial smooth muscle cells: Cloning of distinct subtypes from the internal thoracic artery. *Circ. Res.* **89**, 517–525 (2001).
33. M. Llorian *et al.*, The alternative splicing program of differentiated smooth muscle cells involves concerted non-productive splicing of post-transcriptional regulators. *Nucleic Acids Res.* **44**, 8933–8950 (2016).
34. L. Y. Kong *et al.*, Myotubularin-related protein14 prevents neointima formation and vascular smooth muscle cell proliferation by inhibiting polo-like kinase1. *J. Am. Heart Assoc.* **11**, e026174 (2022).